Bioinspiration & Biomimetics

PAPER

Effects of sensilla morphology on mechanosensory sensitivity in the crayfish

RECEIVED
8 December 2014

REVISED
10 March 2015

ACCEPTED FOR PUBLICATION
23 March 2015

PUBLISHED
24 April 2015

Swapnil Pravin[1], **DeForest Mellon Jr**[2], **Edward J Berger**[3] **and Matthew A Reidenbach**[4]

[1] Department of Mechanical and Aerospace Engineering, University of Virginia, Charlottesville, VA 22904, USA
[2] Department of Biology, University of Virginia, Charlottesville, VA 22904, USA
[3] School of Engineering Education and School of Mechanical Engineering, Purdue University, West Lafayette, IN 47907, USA
[4] Department of Environmental Sciences, University of Virginia, Charlottesville, VA 22904, USA

E-mail: reidenbach@virginia.edu

Keywords: mechanosensing, sensilla, morphology, crayfish

Abstract

Crustaceans contain a great variety of sensilla along their antennules that enable them to sense both hydrodynamic and chemical stimuli in aquatic environments, and can be used to inspire the design of engineered sensing systems. For example, along the antennule of the freshwater crayfish, *Procambarus clarkii*, four predominant mechanosensory sensilla morphologies are found. To study their response to upstream flow perturbations, atomic force microscopy was utilized to determine *P. clarkii* sensilla bending in response to an applied force and a mean torsional stiffness, $k_t = 1 \times 10^{-12}$ N m degree^{-1} was found. A numerical model was developed to quantify the deformation of the four sensilla morphologies due to flow perturbations within their surrounding fluid. These flow perturbations were intended to mimic predator and ambient fluid movements. Results show that upstream fluid motion causes alterations in velocity near the sensilla, accompanied by corresponding variations in pressure along the sensilla surface. The feathered and filamentous sensilla, which are hydrodynamic sensilla, were found to be highly sensitive to flow perturbations. The beaked and asymmetric sensilla, which are bimodal chemo-mechanoreceptors, were found to be much less sensitive to hydrodynamic disturbances. Results also show that sensilla are most sensitive to fluid movement in the along-axis plane of the antennule, with a sharp drop in sensitivity perpendicular to this axis. This sensitivity agrees well with neural responses measured directly from the paired sensory neurons associated with each sensillum. Greater along-axis sensitivity is likely beneficial for determining the direction of fluid movements, which may be important for both aquatic organisms and biomimetic sensing systems.

Introduction

Sensillar morphologies and their structure in aquatic animals play an important role in their sensory function, and can aid in the design of engineered hydrodynamic and chemical sensing systems (Ishida *et al* 2001). Arthropod crustaceans such as crabs, lobsters and crayfish use contact, hydrodynamic, and chemical sensing for a number of activities such as detecting and locating predators, prey, habitat and potential mates (Weissburg 2000, Koehl 2006, Mellon 2012). These organisms inhabit benthic environments, and are often exposed to moving fluids that contain both hydrodynamic and chemical cues. The benthic zone is often highly turbulent, and therefore these organisms are likely to be surrounded by intense gradients in both water velocities and chemical concentrations (Reidenbach and Koehl 2011, Pravin and Reidenbach 2013), which can provide information, but also uncertainty, when detecting and tracking movements of distant odor sources (Moore *et al* 1989, Moore *et al* 1991, Webster and Weissburg 2009). These organisms contain unimodal chemosensitive and hydrodynamically sensitive setae, along with bimodal chemo-mechanosensitive setae that respond to both flows and odors (Koehl 2011, Mellon 2012). These setae can be found along their first antennae, called antennules, in addition to sensilla that are often present over large portions of their body (Mellon 2010, Mellon and Abdul Hamid 2012).

Almost all decapod and stomatopod crustaceans flick their antennules, which facilitates the transport of

odorant molecules to the surface of the olfactory sensilla present on the antennules (Schmitt and Ache 1979, Mead and Koehl 2000, Reidenbach *et al* 2008). Such a motion constitutes a rapid forward-stroke which enhances the movement of odorants through the sensillar hairs, followed by a slower return-stroke which results in odorant laden fluid being trapped between the sensilla (Stacey *et al* 2002, Koehl 2006, Reidenbach *et al* 2008). The entrapped molecules are then transported to the surface of the aesthetascs by small-scale advection and molecular diffusion (Koehl 2006). Price and Ache (1977) and Schmitt and Ache (1979) found that antennular flicking in the spiny lobster *Panulirus argus* enhances the response of olfactory sensory neurons to water-borne odorants, while this flicking breaks down fluid boundary layers that enables for the enhanced delivery of these odorants to chemosensory sensilla (Reidenbach *et al* 2008).

In addition to chemical sensing, sensing of hydrodynamic and mechanical disturbances is also important for detection of predators, mates, and varying environmental substrates (Mellon 2012). There is a rich diversity of sensilla located on antennules of crustaceans, with up to a half-dozen subtypes on a single species (Cate and Derby 2001). The lateral antennular flagellum of the freshwater crayfish, *Procambarus clarkii*, for example, contains a number of subtypes of setae which are all thought to function as olfactory, hydrodynamic, or bimodal mechano-chemosensory sensilla, but the exact functional properties of these structures are not fully known (Mellon 2012).

Arrays of sensory elements, based on the design of biological olfactory sensilla, are often used in the fabrication of robotic noses for sensing odorants in turbulent flow environments. Robots with 'electronic noses' have been employed for tracking of plume sources (Ishida *et al* 2001) as well as type of release (Kikas *et al* 2001a, 2001b, Cantor *et al* 2008), and the intermittency of odorant plumes due to turbulence has been shown to be a key factor in the success of plume tracking. However integration of chemical and hydrodynamic stimuli to aid in search strategy has been less studied. From behavioral studies with aquatic animals as well as design attempts of electronic noses (Ishida *et al* 2005), there is increasing evidence that both chemosensory and hydrodynamic sensory inputs are required to determine odor source location (Atema 1996, Moore and Grills 1999, Gardiner and Atema 2007). Chemical odorants are dispersed throughout aquatic environments through convection and diffusion with the flow and the distribution of odorants across the environment is inherently complex. Being scalar quantities, tracking odorants to their source requires input from other sensory systems as well, such as hydrodynamic sensors in addition to olfactory sensory organs. For *P. clarkii*, local deutocerebral interneurons integrate hydrodynamic and odorant inputs, and the response is enhanced when both flow and odorant stimulation occurs together (Mellon 2005). Both flow and odor signals have been suggested to aid in search behavior (i.e., Atema 1996). Numerous behavioral studies have now shown that hydrodynamic features are important, if not essential, for odor source detection by aquatic vertebrates and invertebrates alike (Weissburg and Zimmer-Faust 1994, Atema 1996, Hodgson and Mathewson 1971, Pohlmann *et al* 2004, Catton *et al* 2007). Hydrodynamic stimulation of the antennules, including flicking (Mellon 2010, Mellon 2012) and from ambient current evokes electrical activity in the central brain neurons (Mellon 2005, Humphrey and Mellon 2007, Mellon and Humphrey 2007). Peak responses of olfactory receptor neurons occur when the aesthetasc responds to a combination of odorant and hydrodynamic stimulus (Grasso and Basil 2002 ,Mellon 2005, Gardiner and Atema 2007). Concentration and flow cues simultaneously excite chemoreceptors and mechanoreceptors of the antennules during flicking. For *P. clarkii*, local deutocerebral interneurons integrate hydrodynamic and odorant inputs, and the response of these central elements is enhanced when both flow and odorant stimulation occurs together (Mellon 2005).

In *P.* clarkii, the kinds of setae found on the lateral antennular flagellum include standing feathered setae, simple asymmetric setae, small and large beaked setae and filamentous setae. Their population density ranges from dense to rare and function varies widely, from highly sensitive near-field reception to bimodal contact chemo-mechanoreception (Cate and Derby 2002a, 2002b, Mellon and Christison-Lagay 2008). Although Mellon and Abdul Hamid (2012) confirmed that weak hydrodynamic stimuli are able to excite the feathered sensilla, the sensitivity of other sensilla morphologies to hydrodynamic disturbance and their functional properties are largely unknown. This study aims to build on the findings of Mellon and Abdul Hamid (2012) on hydrodynamic sensitivity of sensilla in *P. clarkii*. The goal of this study is to determine the effects of hydrodynamic perturbation on flow and pressure distribution near an organism and the structural response of various hydrodynamic sensilla to the perturbation. We also attempt to examine the variation of the response to directionality of the hydrodynamic perturbation and its correlation to nerve spiking thresholds as reported by Mellon and Abdul Hamid (2012). *P. clarkii*, is an ideal model organism to examine antennular sensilla functioning. Its antennules are highly sensitive to water-borne odors and mechanical disturbances and its brain is largely devoted to processing olfactory information (Mellon 2005, Mellon and Humphrey 2007, Mellon *et al* 2014). The specific questions that are addressed in this study are:

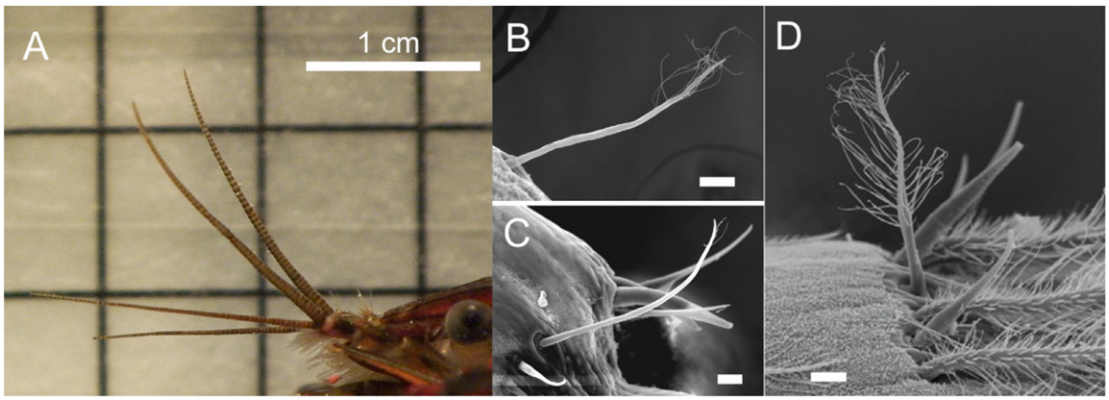

Figure 1. Antennular flagellum and associated mechanosensory sensilla of *P. clarkii*. (A) Lateral and medial antennular flagellum (B) SEM image of the filamentous sensillum (C) SEM image of the beaked sensillum in background, filamentous sensillum in middle, and asymmetric sensillum in foreground. (D) Feathered sensillum, (image modified with permission from Mellon and Abdul Hamid 2012). Scale bar in each image is 20 μm.

Table 1. Dimensions and properties of various morphologies of sensilla found on a crayfish antennule.

Name	Length (μm)	Diameter (μm)	$k_{t,ave}$ (N m degree^{-1})	Sensing mode
Feathered	150	5 tapering to 1		Hydrodynamic
Beaked	150	15 tapering to 5	1×10^{-12}	Hydrodynamic and chemical
Asymmetric	80	10 tapering to 1		Hydrodynamic and chemical
Filamentous	200	10 tapering to 1		Hydrodynamic

(1) What is the effect of upstream perturbation on pressure and velocity around the sensilla of a downstream animal?

(2) What effect does morphology have on force, moment and deformation of sensilla in aquatic organisms?

(3) How does sensilla deformation vary with direction of incoming perturbation?

We utilize atomic force microscopy (AFM) to characterize the torsional stiffness of sensilla and then utilize this information to calculate the response of flow and pressure profiles on the sensilla surface to a pulse of motion upstream using a computational fluid dynamics (CFD) model. The resultant flow profile is applied to the sensilla hairs of four dominant morphologies to examine their structural bending response to the force exerted by the incoming flow. The numerical model and fluid movement matches the same experimental setup used to stimulate near-field mechano-receptors on *P. clarkii* and determine thresholds of sensory neuron responses in Mellon and Abdul Hamid (2012).

Methods

Mechanosensory sensilla morphologies

Scanning electron micrographs (SEM) were obtained from excised lateral antennular flagella of small (5 cm) postmolt or intermolt animals (further described in Mellon and Abdul Hamid 2012). Animals used for imaging were large adult southern swamp crayfish, *Procambarus clarkii*, obtained from a commercial source in Louisiana (Atchafalaya Biological Supply, Raceland, LA, USA). Flagella were removed surgically from the crayfish, and fixed overnight at 4 °C in 2% paraformaldehyde–2% glutaraldehyde in 0.1 mol l^{-1} sodium phosphate buffer (pH 7.4). Fixed flagella were washed 3 times in 0.1 mol l^{-1} phosphate buffer, dehydrated in an ethanol series and critical-point dried prior to being gold coated and imaged on a JEOL 6400 scanning electron microscope (JEOL Ltd, Tokyo, Japan).

The four most dominant morphologies of mechanosensory sensilla (figure 1) found on *P. clarkii* are the feathered, beaked, filamentous, and asymmetric types (Mellon 2012). These four morphologies and their characteristic dimensions, including length, diameter, and hair structure (table 1) were obtained from SEM images. A digital representation of the morphologies of the sensilla were created using computer-aided design from dimensions obtained from the SEM images (figure 2).

Atomic force microscopy

The torsional stiffness k_t for the sensilla was calculated using data from AFM experiments. Samples were prepared in a manner similar to that described above and prepared for in-fluid AFM experiments using a Veeco Multimode AFM. The AFM was first used in contact mode with a fluid cell to probe the sensilla surface and generate a topography. System thermal

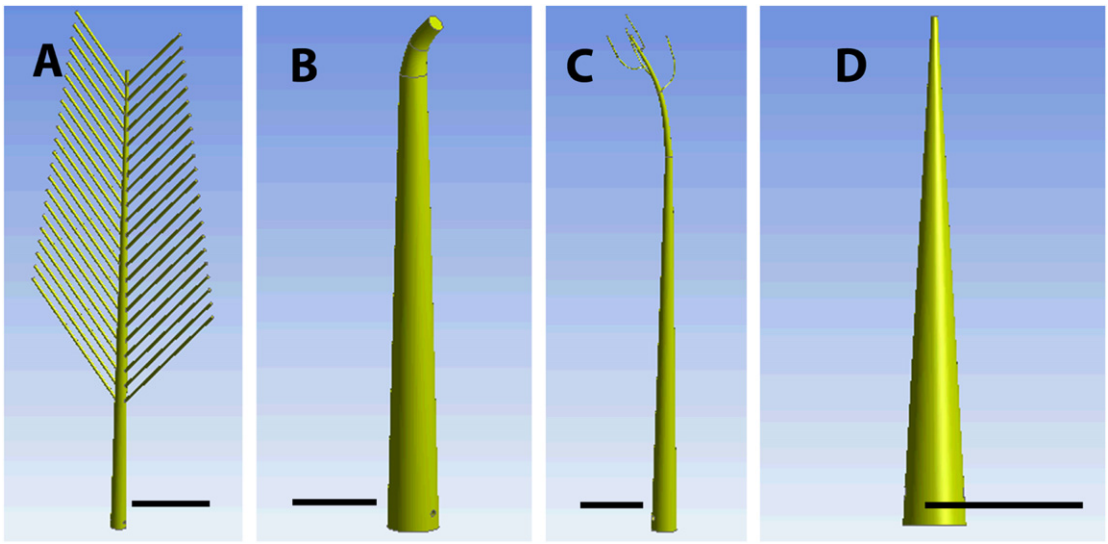

Figure 2. Idealized CAD models of four primary morphologies of sensilla found on crayfish antennules. (A) Feathered, (B) beaked, (C) filamentous and (D) asymmetric sensilla. Scale bar in each image is 25 μm.

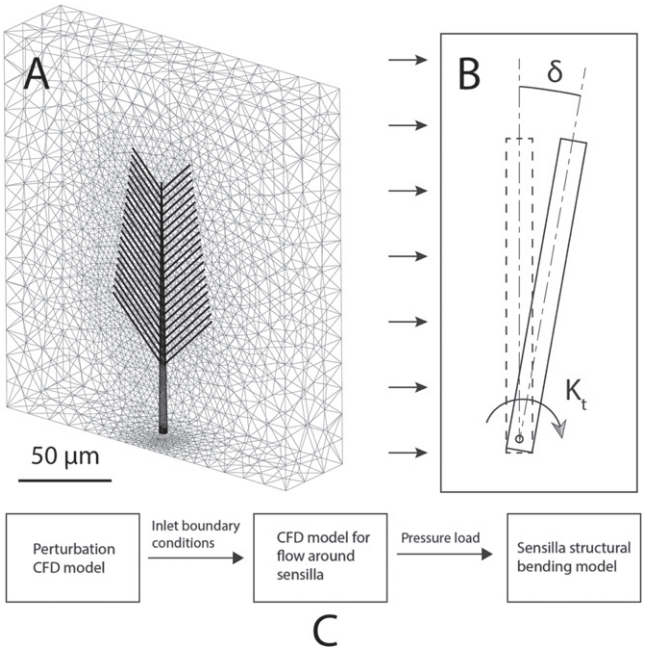

Figure 3. CFD and FSI model of flow surrounding and angular deformation of mechanosensory sensilla. (A) CFD model of the feathered sensilla. Inlet flow into the model is derived from the two-dimensional perturbation model. (B) A revolute joint at the proximal end of the sensilla allows it to rotate around the joint by an angle δ under the pressure of incoming flow. (C) Flowchart for computing the upstream fluid perturbation using the CFD model, which is then used to determine flow and pressure distribution around the sensilla. This pressure load is then inputted into the FSI model to compute angular deflection along the base of the sensilla.

equilibrium was achieved before beginning and a 5×5 μm region was scanned with scan parameters (rate, set-point force, etc) optimized for scan quality. NP-20 probes were used, with nominal cantilever stiffness of 0.06 N m^{-1} and a tip radius of 20–50 nm. Several sets of experiments were performed at different locations on the sensilla, one near the base and one near the distal end, and one more roughly in the middle of the sensilla. Preliminary experiments indicated that the NP-20 probes were appropriate to capture the force and deflection profiles across the range of locations on the sensilla. Across all experiments at all locations, the maximum force observed was on the order of 70 nN, while the maximum cantilever deflection was on the order of 1 μm (corresponding to a maximum sensilla rotation of about 0.05°). The force, F, needed to deflect the sensilla a distance, δ, was quantified for all locations and the angle of rotation was quantified as $\theta_s = L\delta^{-1}$, where L is the moment arm or distance from the proximal end

of the sensilla and small angular deflection is assumed (figure 3). The torsional stiffness was computed using the basic mechanics relation for moment balance at the hinge, assuming the sensilla responded as a rigid body and that the indentation depth was negligible throughout the AFM experiments:

$$k_t \theta_s = FL. \quad (1)$$

The force-deflection data collected at points along the sensilla were essentially linear, suggesting that the assumption of a rigid body rotation hinged at the base is valid. For a small angle of deformation, the torsional stiffness at the base of the sensilla can be quantified as:

$$k_t = FL^2\delta^{-1}. \quad (2)$$

An estimate of $k_t = 1 \times 10^{-12}$ N m degree^{-1} was determined from a subset of the 87 measurements that were made on 11 different sensilla, which varied in length from a minimum of 80 to a maximum of 190 μm. The standard deviation in measurements across all 87 samples was on the order of the mean, mostly due to between-sample variations in physical properties (radius, length) and the challenges of making these kinds of measurements. Aligning the cantilever tip with the axis of the sensilla is challenging, and misalignment surely introduces experimental error due to off-axis loading and potentially slight cantilever twist. The angular rotations expected for the conditions presented in this paper are on the order of 1° or less. The subset of AFM results with maximum rotation near 1° includes 48 of the 87 total measurements, all resulting in torsional stiffness estimates in the range of 1–3 $\times 10^{-12}$ N m degree^{-1}. The torsional stiffness is defined in these simulations as $k_t = 1 \times 10^{-12}$ N m degree^{-1} because this estimate is consistent with the measured data as well as with other measurements of similar hair-like structure torsional stiffnesses (Humphrey *et al* 1993, McConney *et al* 2009, Schaber and Barth 2015). The results presented below also include a sensitivity analysis that explores potential alternative choices for k_t and their impact on hair deflection.

Upstream flow perturbation response

To determine the perturbation in flow and pressure caused by an upstream disturbance, a two-dimensional CFD model of a pulsating flow is employed and the response is recorded adjacent to the antennule surface. A two-dimensional model in used to reduce the computational cost of the simulation and utilize the symmetry of the 3D problem in normal direction to the 2D plane. The ANSYS™ multi-physics software package is used to first solve for the flow and pressure distribution around the antennule, which is then inputted into the fluid-structure interaction model (figure 3). The upstream perturbation was created by a circular object of 9.5 mm diameter (figure 4) and was modeled to mimic the perturbation formed to quantify neural spiking thresholds of standing feathered sensilla by Mellon and Abdul Hamid (2012). In the neural spiking threshold experiments, a 9.5 mm diameter sphere was used to create a flow disturbance, which generated a flow-disturbance pulse which lasted 2 ms. In the model, the circular object was displaced the same distances and over the same time periods as the sphere within the neural spiking threshold experiments.

The model solves for a 2D transient incompressible flow around the sphere and sensilla for which the governing equations are:

$$\frac{\partial u}{\partial t} + u\frac{\partial u}{\partial x} + v\frac{\partial u}{\partial y} = -\frac{1}{\rho}\frac{\partial p}{\partial x} + \upsilon\left(\frac{\partial^2 u}{\partial x^2} + \frac{\partial^2 u}{\partial y^2}\right), \quad (3)$$

$$\frac{\partial v}{\partial t} + u\frac{\partial v}{\partial x} + v\frac{\partial v}{\partial y} = -\frac{1}{\rho}\frac{\partial p}{\partial y} + \upsilon\left(\frac{\partial^2 v}{\partial x^2} + \frac{\partial^2 v}{\partial y^2}\right), \quad (4)$$

where u, v, and p are x-velocity, y-velocity and pressure respectively. The following boundary conditions are applied for the model:

- *Inlet*: $u = U_0$ (1.8 cm s^{-1}, which is the typical flicking speed for crayfish), $v = 0$.
- *Top and bottom*: zero shear slip walls are applied, i.e. $v = 0$, $\partial p/\partial y = 0$, $\partial u/\partial y = 0$.
- *Outlet*: a constant pressure outlet is used: $p = p_{atm.}$
- *Circle walls*: a no-slip wall boundary condition is applied: $u = v = 0$.

A rectangular flow domain of size 200d (d = diameter of the downstream circle) was used. A mesh size of 3500 cells was required to converge the results and capture the flow dynamic for the model. The commercial solver CFX™ was used to solve for velocity and pressure throughout the flow domain. The results from this study are then used as inlet boundary conditions for deformation analysis of the sensilla located on the downstream antennule within the fluid–structure interaction model (figure 3). Figure 3(C) displays the connectivity of models where the results from the perturbation model (figure 4) are used as boundary conditions for the CFD portion of FSI (figure 3(A)). The flow field generated around the sensillum is then applied as a pressure load on the sensillum to compute its deformation around its base, δ (figure 3(B)). This method constitutes a one-way FSI formulation where the flow field around the sensilla affects its structural position but not vice-versa. This formulation is justified since the deflection of the sensilla is small, $\delta \ll 1°$, and hence does not effect the flow field significantly.

The CFD domain in figure 3(A) was generated for each of the four sensilla morphologies. To achieve mesh density convergence, the feathered sensilla flow domain was meshed into ~2 million nodes with tetrahedral dominant elements. The asymmetric, beaked and filamentous models required ~38 000, 24 000 and 370 000 nodes respectively.

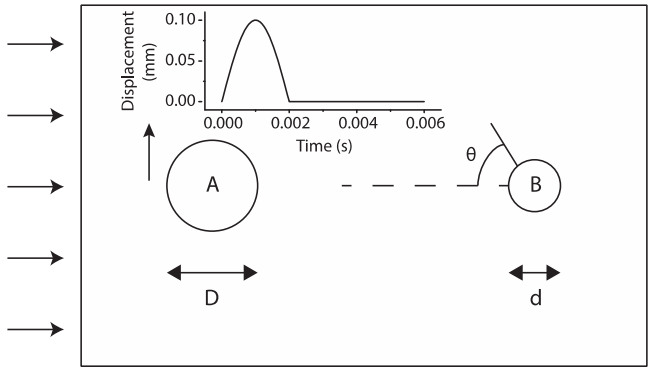

Figure 4. CFD model for velocity and pressure response at the surface of antennule B ($d = 0.5$ mm) caused by a pulse movement of the upstream sphere A ($D = 9.5$ mm). The graph shows the pulse displacement of circle A and the velocity and pressure profile at the sensilla attached to the antennule (circle B) at angle θ are used as inlet conditions for the sensilla CFD models.

Sensilla bending analysis

Within the fluid–structure interaction model, sensilla are assumed to be attached to the antennule at its proximal end by a revolute joint with a torsional stiffness, k_t. The sensillum itself is modeled as a structurally rigid body hinged at its base as a simple torsional spring, since the AFM measurements show little bending along the length of the sensillum. A no-slip wall is applied at the bottom of the flow domain, which is the surface of the antennule. A constant pressure is applied at the outlet and zero shear slip walls are assumed to be present at the remaining three sides. The force and bending moment on the sensillum resulting from the incoming flow are calculated by integrating the resultant pressure over the surface of the sensillum. A steady state analysis for the sensilla bending is performed to calculate the equilibrium deflection of the sensilla structure. Therefore, transient motion is not modeled, and neither inertia nor the mass of the sensilla is assumed to factor in to the final angular position of the sensilla. The effect of relative angular position of the upstream flow perturbation on the sensilla response is determined by adjusting the angular position of the sensillum on the antennule, θ (figure 4) in steps of 20°, and then solving the model for pressure and angle of deflection for each sensillum type.

Results

Upstream perturbation response

The effects of an upstream hydrodynamic perturbation on water velocity and pressure along a *P. clarkii* antennule are studied using a two-dimensional CFD model. The circle upstream undergoes a pulse movement for a duration of 2 ms, as shown in figure 4. Water velocity and pressure are quantified adjacent to the surface of the antennule where a sensillum would normally be present. The Reynolds number for the antennule is ~9 and Re for the sensillum is ~3. The hydrodynamic pulse results in a sharp peak in velocity of 0.85 cm s^{-1} followed by a sharp drop to 0.78 cm s^{-1} before returning to a the mean flow speed of 0.81 cm s^{-1} (figure 5). The peak and the trough in velocity closely correspond to peaks in pressure of 3 and 4 Pa respectively above the background pressure. The results from this model show that a sudden pulse of movement upstream results in a momentary increase in velocity and pressure along the antennule and at locations of mechanosensory sensilla.

Sensilla response to perturbed flow

The flow fields around the various sensillar morphologies are shown in figure 6. The sensillar walls are colored by total displacement of the sensillar surface and the streamlines indicate water velocities at fixed distances from the base for all four morphologies. As the sensilla are attached to the antennule surface through joints, simulated as revolute joints in the FSI model, the sensillum responds to the incoming flow by rotating around the joint by an angle δ. A greater surface area exposed to the flow or a longer length of the sensillum results in larger bending moment applied to it around the joint and resultantly larger angular deformation, δ (figure 7). The filamentous sensilla morphology, which is the longest ($L = 200\ \mu$m) experiences the maximum deformation of 0.91°. This is approximately 66 times greater than the deformation of the asymmetric sensilla morphology, which has the least deformation. The feathered sensilla experiences the maximum total force and bending moment, which is 10 times the force and 23 times the bending moment applied to the asymmetric sensilla. However, the feathered sensillum has less deformation than the filamentous sensillum due to its shorter length. The branching structure of the feathered, and to a lesser extent the filamentous, contributes to the overall drag force creating torque that the sensillum experiences. Due to the low Reynolds number regime of the flow, a greater amount of fluid flows around the feathered sensillum than through its

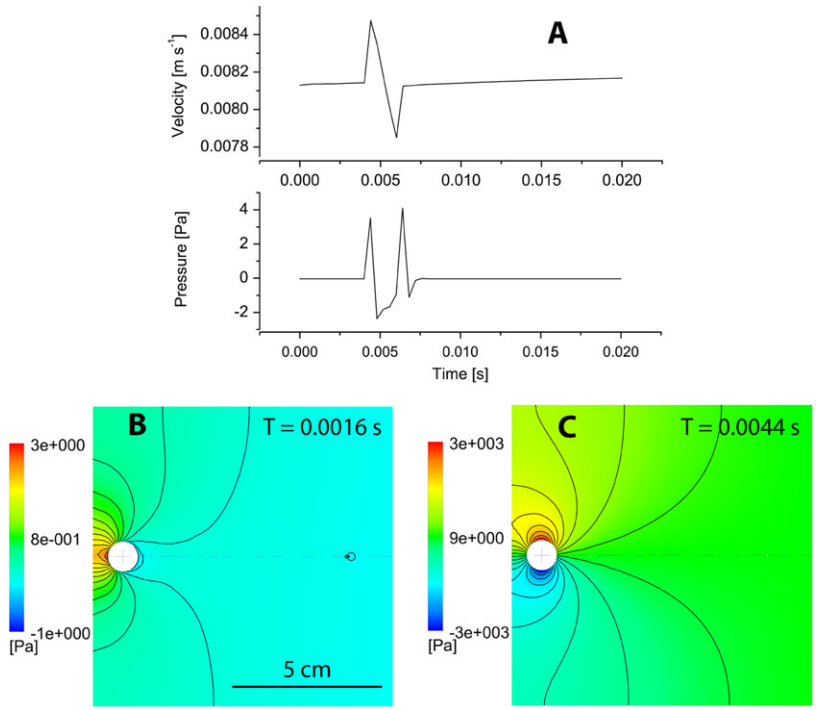

Figure 5. Velocity and pressure response due to an upstream flow perturbation. (A) Velocity and pressure imposed on the sensilla surface caused by movement of 2 ms duration of the upstream sphere. Pressure contours (B) before and (C) after the pulse motion of the upstream circular entity.

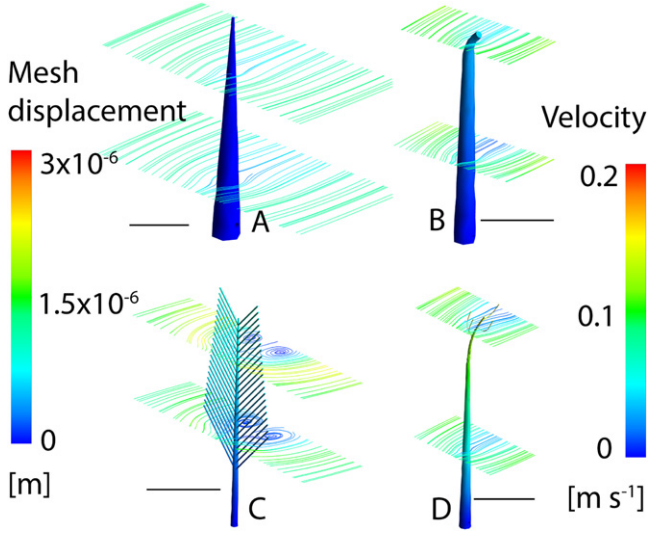

Figure 6. Flow velocity contours and deformation magnitude of the sensilla. (A) Asymmetric sensilla at $z = 20$ and 60 μm, (B) beaked sensilla at $z = 60$ and 140 μm, (C) feathered sensilla at $z = 60$ and 120 μm and (D) filamentous sensilla at $z = 70$ and 190 μm. The contours are colored by velocity and the sensilla surface is colored by magnitude of deformation of the sensilla from its original position.

branches. Such 'paddle-type' behavior (Koehl 2006) provides much greater resistance to the flow.

Direction of perturbation

The effects of the direction of incoming flow perturbation on the sensillar response was determined by varying the flow angle θ (figure 3) from 0° to 360° in increments of 20°. The incoming flow approaches the downstream sensillum at $\theta = 0°$, and $\theta = 180°$ corresponds to the center of its wake. The water velocity around the sensillum increases to a maximum of 1.15 cm s^{-1} as the angle θ increases from 0 to 90° and is the smallest (0.43 cm s^{-1}) at 180° when the flow perturbation approaches the sensillum from the opposite direction (figure 8). The velocities and corresponding pressure distributions along the sensillum have direct correlation to the variation of nerve spike threshold with the direction of perturbation

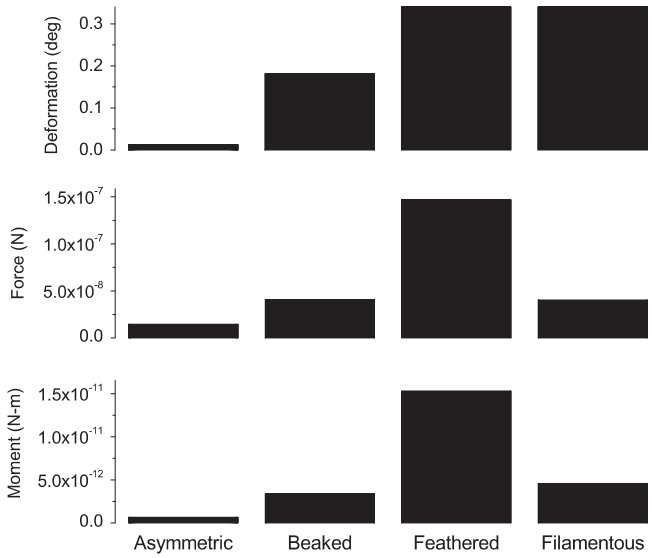

Figure 7. Angular deformation of the sensilla (δ), force exerted by the incoming flow and the corresponding bending moment for different sensilla morphologies.

(figure 9, adapted from Mellon and Abdul Hamid 2012), suggesting that greater perturbations in fluid movement surrounding the antennule, and consequently sensillar deformation δ, lead to increased neural response in the animal's brain. Angular deformation for various sensillar morphologies is compared in figure 10. Results show that deformation variation with direction of perturbation closely follows the flow speed the sensilla are exposed to, with greatest deformation observed in feathered sensilla oriented at right angles to the direction of perturbation.

Model sensitivity to torsional stiffness

An average value of $k_t = 1 \times 10^{-12}$ N m degree^{-1} was used for the models as calculated from AFM measurements for the beaked sensilla. The sensitivity of the model to torsional stiffness for each of the morphologies is determined by varying k_t over several orders of magnitude and calculating the deformation response for each case. Results (figure 11) show that the angular deformation of each of the morphologies is fairly insensitive to changes in torsional stiffness across a range of five orders of magnitude for smaller values of k_t. For stiffness values greater than $k_t = 1 \times 10^{-12}$ N m degree^{-1}, there is a sharp decrease in angular deformation, suggesting that any stiffness greater than that measured from AFM, a reduction in the sensitivity of the sensillum occurs. In addition, there is a transition from the filamentous hairs being the most sensitive at $k_t = 1 \times 10^{-12}$ N m degree^{-1} to the feathered sensilla being the most sensitive to angular deformation at $k_t = 5 \times 10^{-11}$ N m degree^{-1}.

Discussion

Previous studies in the spiny lobster have shown that antennular flicking, either occurring naturally by electrical stimulation via the antennular adductor muscle or by passively generating similar, artificial flicks of the antennule using a pen motor, enhance the responses of individual antennular chemoreceptors to gradients of amino acids (Schmitt and Ache 1979). Furthermore, in the clawed lobster *Homarus americanus* (Gomez and Atema 1996), the optimal integration time for stimulus acquisition in chemosensitive neurons on the antennule is around 200 ms, approximately the time required for the downward phase of an antennular flick. In *P. clarkii*, at least, standing feathered sensilla and perhaps filamentous sensilla can evoke antennular flicking in response to near-field hydrodynamic stimuli (Mellon and Abdul Hamid 2012). One can predict that advection-driven turbulence in the water column may often signal the presence of novel odorants; given the above findings, sampling the environment through aesthetasc sensilla via flicking behavior would therefore appear to be an appropriate, reliable foraging strategy. In this context, it seems important to understand the influence and distribution of flow-fields not only around the aesthetasc (olfactory) sensilla themselves, but also those of neighboring types of sensilla that might modify their immediate kinetic environment.

The results presented in this study show that an upstream perturbation in flow can cause alterations in fluid velocities and the resultant pressure distribution surrounding sensilla along the crayfish antennule. Of the morphologies tested, the standing feathered

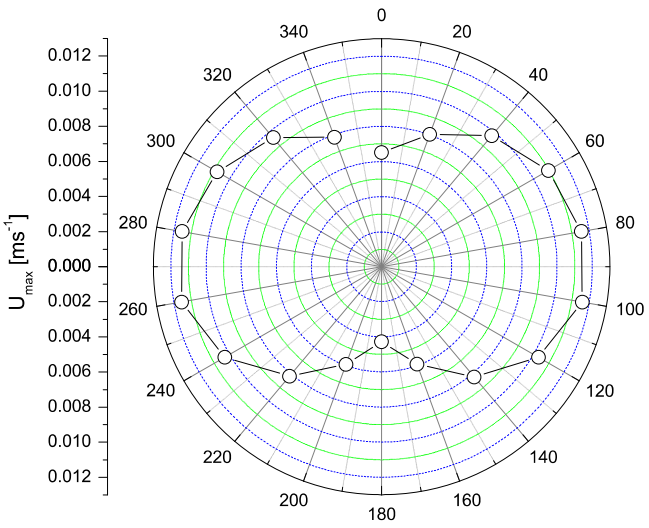

Figure 8. Peak velocity of the incoming flow around the sensilla for various positions, θ around the circumference of the antennule.

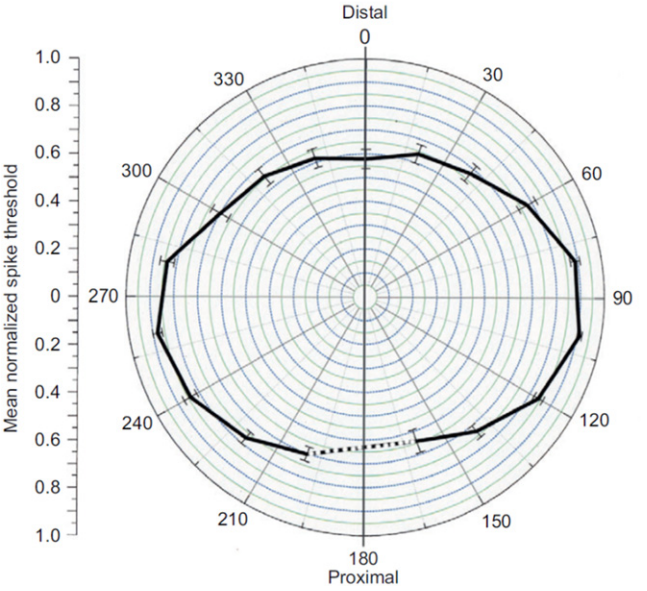

Figure 9. Polar plot of normalized sensillar spiking thresholds in *P. clarkii* as a function of the relative position of a 5 ms near-field stimulus. Data are means ±1 s.e.m. of 25 sensilla. The 0° position was directly ahead of (distal to) the sensillum under observation. The stimulus probe was moved sequentially in 20° increments to 17 different positions clockwise and counterclockwise around the sensillum (adapted with permission from Mellon and Abdul Hamid 2012).

sensillum encounters the largest force and bending moment against the incoming flow while the feathered and filamentous morphology experiences similar but smaller angular deformations. Results also indicate that the sensilla undergo maximum angular deflection when aligned at or close to (depending on the symmetry of the branching structure) right angles to the direction of the perturbation. These hydrodynamic and pressure distribution results are in close conformity to sensitivity to direction of perturbed flow as measured by neuron spiking thresholds in the animal brain as reported in Mellon and Abdul Hamid (2012).

Sensillum morphology and sensitivity

As the upstream perturbation in the flow creates a hydrodynamic disturbance around the antennule, either due to antennule flicking, ambient currents, or turbulence induced by a nearby predator or mate, it generates a pressure distribution along the surface of the sensillum, and causes an angular deformation about its base. Hydrodynamic sensilla have a variety of morphologies that allow varied degrees of sensitivity under different flow conditions. The standing feathered sensillum, due to its large surface area and dense array of branches, generates flow that goes around its

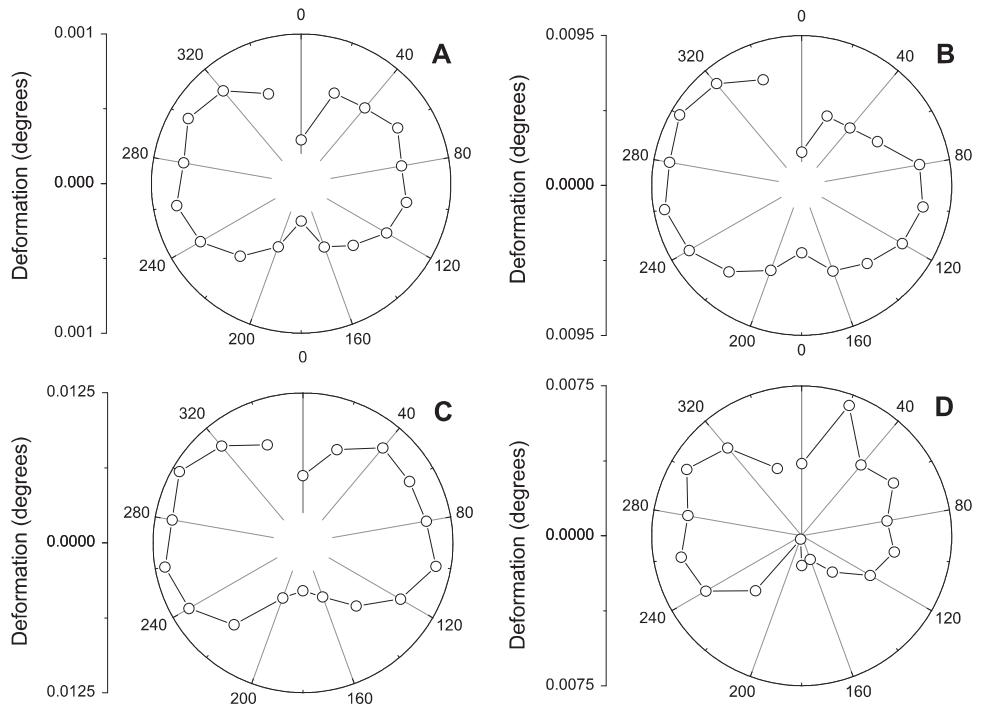

Figure 10. Angular deformation, δ, of the sensilla at positions around the antennule for different sensilla morphologies. (A) Asymmetric (B) beaked (C) feathered and (D) filamentous.

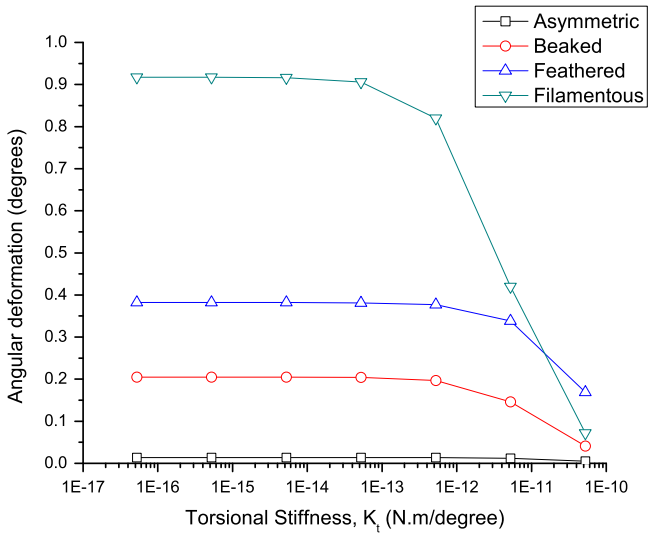

Figure 11. Sensitivity of sensilla deformation to variation in torsional stiffness, k_t. The AFM measurements and value used in the model are for $k_t = 1 \times 10^{-12}$ N m degree^{-1}. The plot shows little variation in deformation (δ) for less stiff sensilla ($k_t < 1 \times 10^{-12}$ N m degree^{-1}) but a sharp reduction in angular deformation, and thus sensitivity of the sensilla to hydrodynamic disturbance, for sensilla that have greater torsional stiffness.

structure instead of through its branches (figure 6). In combination with the low Reynolds number laminar flow it experiences under small fluid perturbations, the feathered sensillum essentially acts as a 'paddle' (Koehl 2006) and experiences the greatest applied fluid force among all predominant sensillar types. However, the bending moment about its base is similar in magnitude to the filamentous sensillum, which experiences less overall force, but due to its greater length, creates an equivalent angular deflection at its base. Both sensillar morphologies result in large deformations around the joint and allow detection of small perturbations in the flow field. The neural response of the feathered sensillum was studied by Mellon and Abdul Hamid (2012) and the greatest extent of deformation around the joint was found to correlate with the direction of largest nerve spiking in the animal brain. This suggests that variations in the magnitude and/or direction of the perturbation can be detected by *P. clarkii*.

Relative sensillum sensitivity and function

Although the feathered sensillum was found to experience the largest force and bending moment, there are many scenarios and environmental conditions in which it would be advantageous to be less sensitive to fluid perturbations, including mechanosensing in high flow environments, mechanosensing during relatively fast antennule flicking, or mechanosensing by direct contact with solid surfaces (Webster and Weissburg 2009, Mellon 2012). These varied functions are performed by the range of sensillar types found on the antennules of crustaceans. The morphology and the fine structure of the aesthetasc sensilla in spiny lobsters and crayfish has been the subject of many studies (Tierney *et al* 1986, Grunert and Ache 1988, Mellon *et al* 1989). During chemical stimulation, these organisms typically exhibit flicking reflexes by their antennules, which initiate rapid antennule movement in the range between 1 and 10 cm s^{-1} (Koehl 2006, Reidenbach *et al* 2008, Nelson *et al* 2013). Therefore, mechanosensors exposed to these rapid accelerations and fluid velocities, in addition to any surrounding ambient currents, must be able to detect and react to this fluid movement occurring at a much higher Reynolds number regime than the fluid perturbations studied. However, input from those sensilla that are most sensitive to water movements may be actively suppressed by the brain through feed-forward inhibition during active flicks (Mellon and Christison-Lagay 2008). In contrast, there is a need to detect and quickly respond to extremely small perturbations in the flow, often caused by predator attacks, and having multiple mechanosensor morphologies with varying sensitivities may play a fundamental role in enabling *P. clarkii* to detect hydrodynamic disturbances. Changes in the magnitude of a flow perturbation or time duration of a perturbation may conceivably alter the transient response of sensilla motion, leading to variations in the angle of deformation. Unfortunately, our model assumes steady state conditions to calculate the equilibrium deflection of sensilla, and a second-order mechanical system would need to be modeled, which includes the effects of mass and inertia, in order to determine transient motion.

Of all the known morphologies on the crayfish antennule, the standing feathered sensilla appear to be the most highly sensitive near-field hydrodynamic receptors (Mellon 2012). They are highly sensitive to hydrodynamic shear providing the first sign of warning for the animal to the possibility of the presence of a predator. The morphology of the sensilla, consisting of a dense array of branches, provides enhanced resistance to the incoming flow, increasing deformation of the sensilla structure at its joint. The beaked sensilla are the second most numerous morphology on the antennules of *P. clarkii*. Their curved tip cuticle has been shown to have permeability to dye crystal violet (Mellon 2012), likely indicating they serve a function in chemical reception. Anatomical studies of similar sensilla in spiny lobsters suggest that these sensilla are bimodal contact chemo-mechanoreceptors (Cate and Derby 2002a, 2002b). Our results show that they have smaller deformational sensitivity (angular deflection in response to flow) than feathered sensilla. These bimodal sensilla can initiate antennule flicking (Mellon 1997) and owing to their lower hydrodynamic sensitivity, their mechanosensing function may be active during the flick to aid in chemical detection, however their specific function is still unknown. Neither is the function of asymmetric and filamentous setae in *P. clarkii* established. The asymmetric sensilla have been inferred to be bimodal chemo-mechanoreceptor in lobsters (Cate and Derby 2002a). They show the least sensitivity to flow-field perturbation in our results. Although their function is speculative, their low sensitivity allows them to respond either to fast water movements, such as during a flick, or act as contact sensilla. Filamentous setae are present in sparse population on the antennules on *P. clarkii*. These sensilla are the longest in length among all the sensillar morphologies tested in this study and have a group of filamentous projections near their tip, which provides a large angular deflection. Likely, their primary function is hydrodynamic sensing, as suggested earlier by Mellon (2012), but it is unknown if they aid in chemosensing. Although the ultimate functioning of these various morphologies is unknown, it is likely that they all serve specific functions in the detection of their surrounding fluid environment. Further research in electrophysiology and brain response of the animals to stimulation of these sensilla, combined with numerical models that can elucidate the magnitude of perturbation required for hydrodynamic detection, can help achieve a greater understanding of their role in detecting hydrodynamic and chemical stimuli.

Role of hydrodynamic sensing in plume tracking

In aquatic benthic environments, flow fields are often turbulent and the distribution of diffusing odorants is intermittent and complex. The interwoven spatial and temporal structure of the flow and chemical distribution indicates that instantaneous sensing of the flow field can be of crucial importance in chemical sensing (Pravin and Reidenbach 2013). Antennule flicking enhances the odorant diffusion to the sensilla surface (Pravin *et al* 2012) and allows it to enter the permeable cuticle on the aesthetasc surface before it comes in contact with the ORN dendrites. Although it has been shown that flow and chemical signal integration in the form of odorant flux can enhance the animal's ability to locate the source of a chemical plume (Gardiner and Atema 2010), how and to what extent an animal integrates hydrodynamic and chemical information is currently unknown. Results from Pravin and Reidenbach (2013) have shown that mean odorant concentration and intermittency in the odorant signal

increase towards the plume source, but the temporal and spatial rate of this increase is slow. Long measurement times would be necessary to be useful for chemosensory guidance if odorant concentration were used alone (Reidenbach and Koehl 2011). However, odorant fluxes measured transverse to the mean flow direction, measured as the simultaneous instantaneous fluctuation in concentration and velocity, have been shown to have statistically distinct magnitude and directional information. This information is spatially distinct on either side of a plume centerline, and can be determined with sampling times of 0.5 s or less. Aquatic animals typically have neural responses to odorant and velocity fields at rates between 50 and 500 ms (Marschall and Ache 1989, Gomez and Atema 1996, Derby *et al* 2001, Mellon *et al* 2014), suggesting this simultaneous sampling of both flow and concentration can be highly beneficial for rapid detection and movement towards the source of the odorant plume. This suggests that in the use of biologically inspired electronic noses, integration of hydrodynamic and chemical stimuli on time scales similar to neural response times of organisms (50–500 ms), may enhance both the success of a search and time to finding the source. Our findings also suggest that due to the varying sensitivity of the mechanosensilla to angle of hydrodynamic perturbation, these sensilla can be used to determine the direction of flow disturbance. As chemical signals become entrained by turbulence and mixed within the plume as they propagate downstream, sensing both odor concentration and direction from which these 'flavored eddies' (Atema 1996) originated from, can greatly enhance information input about source location.

Hydrodynamic stimulation of feathered sensilla show that they are sensitive to impulsive stimuli originating close to the axial plane of the flagellum (Mellon and Christison-Lagay 2008, Mellon and Abdul Hamid 2012). An examination of the SEM images of the sockets of feathered sensilla also reveals that there are preferred directional sensitivities, which are most sensitive at right angles to the hinge-like elongation of the sensillar base. Mellon and Abdul Hamid (2012) reported that the differences in fluid directional sensitivities were not significant for detection by standing feathered sensilla, except for a definite drop close to 180° opposite the preferred direction. However, through an ANOVA analysis of the data, they showed highly significant differences in response threshold at different angles with reference to the sensilla ($P < 0.001$). The results shown in this numerical study indicate slightly increased angular deflection of the sensilla for perturbations at right angles to the sensilla orientation and also a drop in deformation at 180° to the preferred direction. This indicates that the sensilla although they are sensitive to direction of perturbation, retain their sensitivity from almost all directions except at $\theta = 180°$, when the flow movement occurs directly behind the sensillar orientation.

In conclusion, a rich diversity of morphologies is found among sensilla on the antennules of a crayfish. These morphologic variations may allow *P. clarkii* to detect both small and large perturbations under different flow conditions and, combined with chemoreceptor aesthetascs, provide the ability for integration of flow and chemical stimuli on relevant time and spatial scales to effectively navigate their benthic environment. These same characteristics may also improve the design of engineered sensors for the detection and tracking of chemicals in aquatic environments.

Acknowledgments

We are grateful to our colleague, the late Professor J A C Humphrey, for insightful discussions regarding flicking behavior and mechanosensing in crayfish. This research was funded by the National Science Foundation grant NSF-CBET-0933034.

References

Atema J 1996 Eddy chemotaxis and odor landscapes: exploration of nature with animal sensors *Biol. Bull.* **191** 129–38

Cantor R S, Ishida H and Janata J 2008 Sensing array for coherence analysis of modulated aquatic chemical plumes *Anal. Chem.* **80** 1012–8

Cate H S and Derby C D 2001 Morphology and distribution of setae on the antennules of the Caribbean spiny lobster *Panulirus argus* reveal new types of bimodal chemo-mechano-sensilla *Cell Tissue Res.* **304** 439–545

Cate H S and Derby C D 2002a Hooded sensilla homologues: structural variations of a widely distributed bimodal chemomechanosensillum *J. Comp. Neurology* **444** 345–57

Cate H S and Derby C D 2002b Ultrastructure and physiology of the hooded sensillum a bimodal chemo-mechanosensillum of lobsters *J. Comp. Neurology* **442** 293–307

Catton K B, Webster DR, Brown J and Yen J 2007 Quantitative analysis of tethered and free-swimming copepodid flow fields *J. Exp. Biol.* **210** 299–310

Derby C D, Steullet P, Horner A J and Cate H S 2001 The sensory basis of feeding behaviour in the Caribbean spiny lobster *Panulirus argus Mar. Freshw. Res.* **52** 1339–50

Gardiner J M and Atema J 2007 Sharks need the lateral line to locate odor sources: rheotaxis and eddy chemotaxis *J. Exp. Biol.* **210** 1925–34

Gardiner J M and Atema J 2010 The function of bilateral odor arrival time differences in olfactory orientation of sharks *Curr. Biol.* **20** 1187–91

Gomez G and Atema J 1996 Temporal resolution in olfaction II: time course of recovery from adaptation in lobster chemoreceptor cells *J. Neurophysiol.* **76** 1340–3

Grasso F W and Basil J A 2002 How lobsters crayfishes and crabs locate sources of odor: current perspectives and future directions *Curr. Opin. Neurobiol.* **12** 721–7

Grunert U and Ache B W 1988 Ultrastructure of the aesthetasc (olfactory) sensilla of the spiny lobster Panulirus argus *Cell Tissue Res.* **251** 95–103

Hodgson E S and Mathewson R F 1971 Chemosensory orientation in sharks *Ann. New York Acad. Sci.* **188** 175–81

Humphrey J A C, Devarakonda R, Iglesias I and Barth F G 1993 Dynamics of arthropod filiform hairs: I. Mathematical modelling of the hair and air motion *Phil. Trans. R. Soc.* B **340** 423–44

Humphrey J A C and Mellon D Jr 2007 Analytical and numerical investigation of the flow past the lateral antennular flagellum of the crayfish *Procambarus clarkii J. Exp. Biol.* **210** 2969–78

Ishida H, Nakamoto T, Moriizumi T, Kikas T and Janata J 2001 Plume-tracking robots: a new application of chemical sensors *Biol. Bull.* **200** 222–6

Ishida H, Nakayama G, Nakamoto T and Moriizumi T 2005 Controlling a gas/odor plume-tracking robot based on transient responses of gas sensors *IEEE Sensors J.* **5** 537–45

Kikas T, Ishida H, Webster D R and Janata J 2001a Chemical plume tracking: I. Chemical information encoding *Anal. Chem.* **73** 3662–8

Kikas T, Janata P, Ishida H and Janata J 2001b Chemical plume tracking: II. Multiple-frequency modulation *Anal. Chem.* **73** 3669–73

Koehl M A R 2006 The fluid mechanics of arthropod sniffing in turbulent odor plumes *Chem. Senses.* **31** 93–105

Koehl M A R 2011 Hydrodynamics of sniffing by crustaceans *Chemical Communication in Crustaceans* ed T Breithaupt and M Theil (Berlin: Springer) pp 85–102

Marschall H P and Ache B W 1989 Response dynamics of lobster olfactory neurons during simulated natural sampling *Chem. Senses* **14** 725

McConney M E, Schaber C F, Julian M D, Eberhardt W C, Humphrey J A, Barth F G and Tsukruk V V 2009 Surface force spectroscopic point load measurements and viscoelastic modelling of the micromechanical properties of air flow sensitive hairs of a spider (*Cupiennius salei*) *J. R. Soc. Interface* **6** 681–94

Mead K S and Koehl M A R 2000 Stomatopod antennule design: the asymmetry sampling efficiency and ontogeny of olfactory flicking *J. Exp. Biol.* **203** 3795–808

Mellon D 1997 Physiological characterization of antennular flicking reflexes in the crayfish *J. Comp. Physiol.* A **180** 553–65

Mellon D 2005 Integration of hydrodynamic and odorant inputs by local interneurons of the crayfish deutocerebrum *J. Exp. Biol.* **208** 3711–20

Mellon D 2010 Regulation of axonal conduction velocity from hydrodynamic sensilla on the crayfish antennule *J. Exp. Biol.* **213** 3778–86

Mellon D 2012 Smelling feeling tasting and touching: behavioral and neural integration of antennular chemosensory and mechanosensory inputs in the crayfish *J. Exp. Biol.* **215** 2163–72

Mellon D and Abdul Hamid O A 2012 Identified antennular near-field receptors trigger reflex flicking in the crayfish *J. Exp. Biol.* **215** 1559–66

Mellon D and Christison-Lagay K 2008 A mechanism for neuronal coincidence revealed in the crayfish antennule *Proc. Natl Acad. Sci.* **105** 14626–31

Mellon D and Humphrey J A 2007 Directional asymmetry in responses of local interneurons in the crayfish deutocerebrum to hydrodynamic stimulation of the lateral antennular flagellum *J. Exp. Biol.* **210** 2961–8

Mellon D, Pravin S and Reidenbach M A 2014 A nose too far: regional differences in olfactory receptor neuron efficacy along the crayfish antennule *Biol. Bull.* **227** 40–50

Mellon D, Tuten H R and Redick J 1989 Distribution of radioactive leucine following uptake by olfactory sensory neurons in normal and heteromorphic crayfish antennules *J. Comp. Neurology* **280** 645–62

Moore P A, Gerhardt G A and Atema J 1989 High resolution spatio-temporal analysis of aquatic chemical signals using microelectrochemical electrodes *Chem. Senses* **14** 829–40

Moore P A and Grills J L 1999 Chemical orientation to food by the crayfish *Orconectes rusticus*: influence of hydrodynamics *Animal Behav.* **58** 953–63

Moore P A, Scholz N and Atema J 1991 Chemical orientation of lobsters, *Homarus americanus*, in turbulent odor plumes *J. Chem. Ecol.* **17** 1293–307

Nelson J M, Mellon D and Reidenbach M A 2013 Effects of antennule morphology and flicking kinematics on flow and odor sampling by the freshwater crayfish *Procambarus clarkii* *Chem. Senses* **38** 729–41

Pohlmann K, Atema J and Breithaupt T 2004 The importance of the lateral line in nocturnal predation of piscivorous catfish *J. Exp. Biol.* **207** 2971–8

Pravin S, Mellon D and Reidenbach M A 2012 Micro-scale fluid and odorant transport to antennules of the crayfish *Procambarus clarkii J. Comp. Physiol.* A **198** 669–81

Pravin S and Reidenbach M A 2013 Simultaneous sampling of flow and odorants by crustaceans can aid searches within a turbulent plume *Sensors* **13** 16591–610

Price R and Ache B W 1977 Peripheral modification of chemosensory information in the spiny lobster *J. Comp. Physiol.* A **57** 249–53

Reidenbach M A, George N T and Koehl M A R 2008 Antennule morphology and flicking kinematics facilitate odor sampling by the spiny lobster *Panulirus argus J. Exp. Biol.* **211** 2849–58

Reidenbach M A and Koehl M A R 2011 The spatial and temporal patterns of odors sampled by lobsters and crabs in a turbulent plume *J. Exp. Biol.* **214** 3138–53

Schaber C and Barth F 2015 Spider joint hair sensilla: adaptation to proprioreceptive stimulation *J. Comp. Physiol.* A **201** 235–48

Schmitt B C and Ache B W 1979 Olfaction: responses of a decapod crustacean are enhanced by flicking *Science* **205** 204–6

Stacey M T, Mead K S and Koehl M A R 2002 Molecule capture by olfactory antennules: mantis shrimp *J. Math. Biol.* **44** 1–30

Tierney A J, Thompson C S and Dunham D W 1986 Fine structure of aesthetasc chemoreceptors in the crayfish *Orconectes propinquus Can. J. Zool.* **64** 392–9

Webster D R and Weissburg M J 2009 The hydrodynamics of chemical cues among aquatic organisms *Annu. Rev. Fluid Mech.* **41** 73–90

Weissburg M J 2000 The fluid dynamical context of chemosensory behavior *Biol. Bull.* **198** 188–202

Weissburg M J and Zimmer-Faust R K 1994 Odor plumes and how blue crabs use them to find prey *J. Exp. Biol.* **197** 349–75